AIP | Applied Physics Letters

Flow and force inducement using micron size dielectric barrier discharge actuators

Justin C. Zito, Ryan J. Durscher, Jignesh Soni, Subrata Roy, and David P. Arnold

Citation: Appl. Phys. Lett. **100**, 193502 (2012); doi: 10.1063/1.4712068
View online: http://dx.doi.org/10.1063/1.4712068
View Table of Contents: http://apl.aip.org/resource/1/APPLAB/v100/i19
Published by the American Institute of Physics.

Flow and force inducement using micron size dielectric barrier discharge actuators

Justin C. Zito,[1] Ryan J. Durscher,[2] Jignesh Soni,[2] Subrata Roy,[2,a)] and David P. Arnold[1]
[1]*Interdisciplinary Microsystems Group, Department of Electrical & Computer Engineering, University of Florida, Gainesville, Florida 32611, USA*
[2]*Applied Physics Research Group, Department of Mechanical & Aerospace Engineering, University of Florida, Gainesville, Florida 32611, USA*

(Received 15 March 2012; accepted 18 April 2012; published online 8 May 2012)

Micron size dielectric barrier discharge actuators, designed for minimal footprint area and weight penalty, show a wall jet up to 2.0 m/s consuming 15 W/m of electrode. A torsional balance measures force up to 3 mN/m of electrode and demonstrates equivalent "thrust effectiveness" (induced force/power) to macroscale actuators. Compared with reported macroscale data, the microscale actuator shows a 31% increase in energy conversion efficiency. Per unit actuator mass, both the force and the velocity induced by microscale actuators show an order of magnitude (22.1 and 18.5 times, respectively) increase over macroscale actuators, making them suitable for distributed flow control applications. © *2012 American Institute of Physics*. [http://dx.doi.org/10.1063/1.4712068]

For active flow control applications, dielectric barrier discharge (DBD) devices offer the advantages of lack of moving parts, surface compliance, fast response, and ease of construction, but generally suffer from low flow control authority (i.e., induced flow velocity, momentum transfer, and thrust). Conventional DBD devices consist of two offset electrodes on either side of a dielectric material. With high-voltage pulsed or AC excitation, the gas locally above the dielectric becomes weakly ionized creating a plasma discharge. This plasma imparts an electrohydrodynamic (EHD) force on the surrounding fluid, inducing a 1–4 m/s wall jet occurring 0.5–1 mm above the dielectric surface. The net thrust produced ranges from a few mN/m to over 150 mN/m (thrust per unit length electrode), and the power consumption can range up to ~650 W/m, depending on both input voltage and frequency and the actuator geometry.[1] The actuator's "effectiveness"–output per consumed power–is a useful metric for comparing different designs operated at different voltage levels and frequencies. We apply this metric for both 'velocity effectiveness' (velocity divided by power) and 'thrust effectiveness' (force divided by power) of DBD plasma actuators. In the case where thrust, velocity, and power data are all reported, the actuator's energy conversion efficiency is computed.

The EHD force density ($\mathbf{F}$) is a product of the applied electric field ($\mathbf{E}$) and the net separated space charge density (q), $\mathbf{F} = q\mathbf{E}$. The fluidic control authority of the actuator is dependent on this force density and may be improved by increasing either the applied field or the space charge density. However, the bulk of the plasma is quasi neutral and, therefore, space charge limited, whereas in the sheath, Debye shielding[2] is prevalent and large charge separations can accrue. This implies that the primary contribution to the force is generated within the space charge separated sheath. Wang *et al.*[3] demonstrated computationally that the plasma sheath begins to dominate the plasma volume as the electrode gap is decreased below ~10 μm. A 10–100× increase in the induced force density was predicted. By reducing the actuator dimensions, a larger percentage of the energy expended may be focused within the space charge separated sheath, resulting in a more efficient momentum transfer to the surrounding gas.

Furthermore, the force density may be increased by increasing the electric field, $\mathbf{E}$. This may be accomplished by simply increasing the voltage, reducing the dielectric thickness, or through geometric manipulation of the exposed electrode. Reducing the dielectric layer thickness increases the electric field resulting in an increase in measured thrust[1] (for a given input voltage/frequency). Abe *et al.*[4] found an increase in the momentum transferred though the use of thinner copper tape electrodes. Similarly, Hoskinson *et al.*[5] demonstrated an exponential increase in measured thrust as the diameter of the wire electrode decreased from 0.40 mm to 0.11 mm. These dramatic increases may be explained by considering the electric field around a conducting wire: For a cylindrical conductor at a given potential, the electric field strength is inversely proportional to the wire's radius ($|\mathbf{E}| \propto 1/r$). Hence, fine-scale electrodes may provide an effective method for increasing the force density.

Through miniaturization of the DBD actuator geometries (both electrode size and electrode gap), we aim to leverage both an increase in electric field and charge separation in an effort to improve the fluidic control authority and actuator effectiveness. In this Letter, we demonstrate the fabrication of microscale DBD devices and experimentally analyze their power consumption, velocity distribution, and thrust production with reduced-scale geometries.

The devices are constructed using 10 mm long (spanwise dimension) thin-film titanium electrodes and a 10 μm thick polyimide dielectric on glass substrates (500 μm thick) using semiconductor fabrication techniques.[6] The electrodes are created using sputter deposition, and the polyimide layer is spin-coated and heat-cured. The powered (top) electrodes are 1 μm thick and range from 10 μm to 500 μm in width (streamwise dimension). The ground (bottom) electrodes are 0.1 μm thick and range from 10 μm to 1 mm in width. All

a)Electronic mail: roy@ufl.edu. URL: http://cpdlt.mae.ufl.edu/roy/.

devices have a 100 μm gap between the electrodes. Fig. 1 shows a single device used in these experiments (a) as well as a cross-sectional schematic providing the actuator dimensions (b).

For testing, a high-voltage sinusoidal input at 1 kHz is generated using a function generator and amplifier (Trek 30/20A). A high-voltage probe measures the voltage amplitude across the actuator terminals, and a current monitor is used for current measurements at the input (high-voltage side) of the actuator. A digital oscilloscope captures both of these signals, and the average power dissipated is computed by integrating the voltage-current product over 200 periods.

Particle image velocimetry (PIV) is used to measure the instantaneous velocities induced by the plasma discharge. The PIV setup consists of a Nd:YAG laser (New Wave Research) and uses a CCD camera (LaVision Imager Pro X 4M) with a 105 mm macro lens. The laser sheet is approximately 1 mm thick and is positioned at the mid-point of the electrodes. Ondina oil is used for the PIV seed material, having a mean particle diameter of 0.8 μm. The velocity field is time-averaged over 80 image pairs with a spatial resolution of 78.6 μm for a 20 mm wide field-of-view.

Pitot measurements are used to verify the PIV data, using a glass pipette probe with 1.5 mm outer diameter and 1.0 mm inner diameter. A differential pressure transducer having a full-scale pressure range of ± 9 Pa with accuracy of 0.01 Pa is used to measure the stagnation pressure. The measured pressure is converted to velocity using Bernoulli's principle. A traverse system allows precise control for incrementing the probe location. The absolute position relative to the substrate, however, is limited in accuracy by the initial manual alignment.

Direct force measurement is performed using a torsional balance, which measures the plasma actuator thrust as an angular deflection acting in opposition to torsion springs. The displacement is measured using a reflectance-based optical displacement sensor (PhilTec D100) having 40 nm resolution. The balance is calibrated using an electrostatic force between parallel plate electrodes, which is presumed "known" via finite-element computation using ANSYS MAXWELL 2D electromagnetic field simulation software. A similar torsional balance for microNewton thrust measurements is provided by Germer-Castano.[7] The rotational spring constant obtained through electrostatic calibration is validated using log decrement analysis, and a viscous oil bath is used to damp out extraneous vibrations to facilitate force measurements with an estimated resolution of 35 nN.

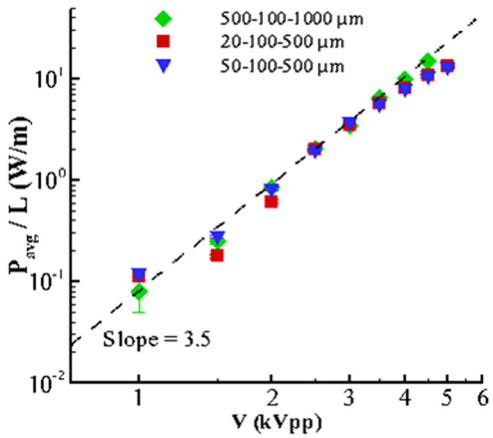

FIG. 2. Logarithmic plot of power consumed for DBD devices with varying electrode geometries and operated at 1 kHz. The nomenclature corresponds to the width of the powered electrode, electrode gap, and grounded electrode, respectively.

Fig. 2 shows the power consumed for microscale DBD devices with varying electrode widths operated at 1 kHz. The power consumption shows little dependency on the exposed electrode width. However, slight differences are observed for the grounded electrode width; a wider ground electrode slightly increases the power dissipation. For macroscale actuators, the electrical power consumed scales exponentially with the sinusoidal input voltage amplitude,[8] $P \propto V^{\alpha}$ with $\alpha \approx 3.5$. The data in Fig. 2 are fit with a power-law to examine the dependency of power on the applied voltage. In logarithmic scale, the slope of the dashed fit line indicates the power scales exponentially with the voltage, with the exponent $\alpha = 3.5$ in these data. The average power consumed reaches 15 W/m at 5 kV_{pp} and 1 kHz.

PIV data are shown in Fig. 3 for a microscale DBD actuator with a 10 μm wide exposed electrode and 1 mm wide ground electrode. The velocity magnitude reaches up to 2 m/s

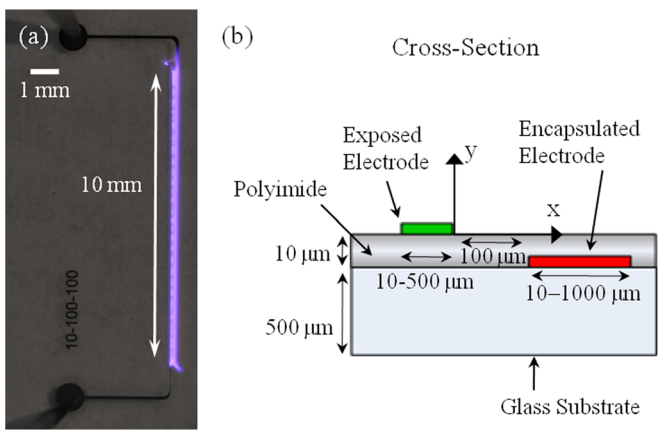

FIG. 1. (a) Top view of device used for experimental data (shown during discharge). The nomenclature corresponds to the width of the powered electrode, electrode gap, and grounded electrode, respectively. (b) Cross-section schematic showing details of the device geometry.

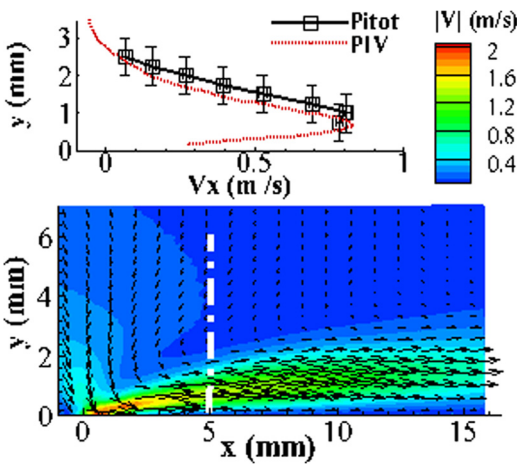

FIG. 3. PIV data for device with a 10 μm wide powered electrode and a 1 mm wide grounded electrode. The upper plot gives the velocity profile from pitot measurements at x = 5 mm downstream.

in the region near the electrodes, and a wall jet is established that extends over 15 mm downstream. The wall jet is similar in profile to those produced using macroscale DBD actuators. To validate the PIV results, pitot measurements were made 5 mm downstream from the edge of the powered electrode (location indicated with dashed vertical line). The top plot in Fig. 3 compares the results from the velocity computed from pitot measurements with an extracted profile from PIV data. The pitot measurements show good agreement with the PIV data, with slight discrepancy between the vertical location of the data points. The offset between the two measurements is most likely attributed to the 1 mm diameter of the pitot tube over which the pressure measurement is averaged, as well as the initial manual alignment.

Measurements from the torsion balance force tests are shown in Fig. 4 for an actuator with a 10 μm wide powered electrode and 100 μm wide ground electrode. The plot shows the optically measured displacement as a function of time for various plasma excitations. Calibration measurements are made using built-in calibration electrodes for pre- and post-experiment comparison. The first two pulses correspond with a 50 V and 100 V potential applied across the calibration electrodes, providing electrostatic force and causing the balance to deflect toward the fixed electrode (away from the sensor). Following the calibration pulses, the actuator is successively stepped up in voltage from 4 to 6.5 kV_{pp} in 0.5 kV_{pp} increments. Each voltage is applied for approximately 10 s before turning off the actuator. Post actuator calibration provides increased resolution over the range of the displacements measured using the actuator.

Using the measured deflections from the DBD actuator and comparing with the calibration measurements, the thrust is extracted for the different excitation voltages. Fig. 5 plots the average thrust in logarithmic scale against applied voltage for three actuators having different ground electrode widths. The device with a 1 mm wide ground electrode produced the greatest force, up to 3 mN/m. As observed in the power consumption data, devices with wider ground electrodes consumed slightly more power, which follows along with the increase in force observed for the device with the largest ground electrode.

The results from the microscale actuators are compared with reported[1,4,9] macroscale DBD actuator performance and summarized in Table I. The actuator volume and mass are computed based on the DBD materials and geometries provided in each reference, with electrode length normalized to

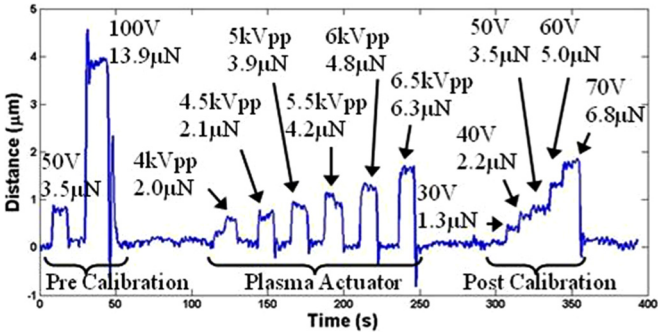

FIG. 4. Displacement measurements from torsional force balance for a microscale DBD actuator. Electrostatic calibration is performed before and after each actuator tested using parallel plate electrodes.

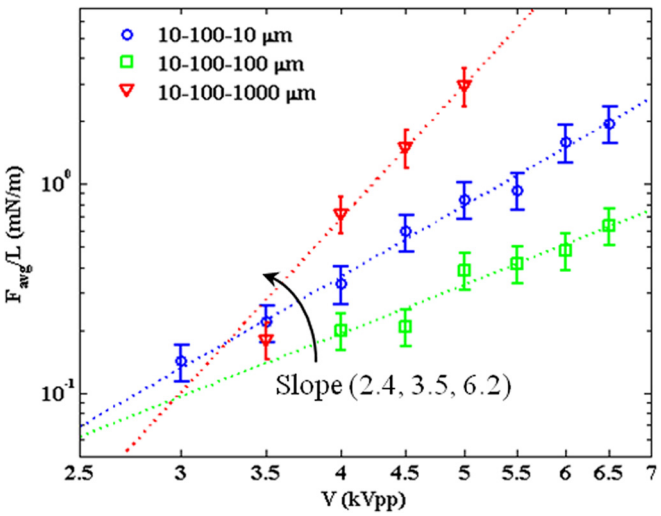

FIG. 5. Logarithmic plot of the average thrust measured for three actuators having different ground electrode widths. The devices all have 10 μm wide exposed electrodes and a 100 μm gap. Thrust normalized by the electrode length ($l = 10$ mm).

1 m. The first row reports the actuator thrust effectiveness; here, one of the two macroscale actuators[4] indicate similar thrust and power values to the microscale actuator, and the other macroscale device[1] indicates significantly larger thrust and power values. However, all three cases demonstrate equivalent thrust effectiveness. The fourth row reports the velocity effectiveness; the microscale actuator provides a 63% increase in velocity effectiveness compared with Forte *et al.*,[9] and 86% increase compared with Abe *et al.*[4]

The bottom row in Table I provides the energy conversion efficiency ϵ for the cases where both velocity and thrust data are reported. The efficiency is computed using the mean force, peak velocity, and average power consumption values, $\epsilon = F_x v_{max}/P_{avg}$. The microscale actuator provides a 31% increase in efficiency compared with Abe *et al.*[4] On a per-volume or per-mass basis, the micro actuators out-perform the macro actuators in both thrust and velocity metrics. This is attributed to the extreme size reduction of the microscale devices, in addition to the reduction in power consumption. The thick dielectric layer (few millimeters) generally utilized for macro DBD actuators governs the voltage, and in-turn, the power required to generate a wall jet. Employment of an ultra-thin dielectric layer (10 μm) and miniaturized electrodes allows the micro actuator to produce velocities on the order of macroscale actuators with a significant reduction in the power, size, and mass.

To further improve the actuator thrust effectiveness and thrust density (force per actuator volume), the dielectric gap should be reduced from 100 μm as reported here to a few microns.[3] At atmospheric pressure and room temperature, the Debye length for DBD plasma is on the order of 1 μm (for $T_e = 3$ eV, $n_e = 10^{20}$ m^{-3}, where T_e and n_e are the electron temperature and electron number density, respectively[10]), occupying just 1% of the electrode gap. With reduced electrode separation, the Debye length (region of space-charge separation) will occupy a larger portion of the discharge region where the force contribution is greatest.

In conclusion, we have demonstrated the operation, flow inducement, and thrust generation of DBD devices having

TABLE I. Micro- and macro-DBD actuator performance metrics; comparing actuator thrust and velocity to power consumption, device geometry, and material properties.

Performance metrics	Micro-DBD $v_{max} = 2$ m/s and $F_x = 3$ mN/m $P_{avg} = 15$ W/m $V = 5\,kV_{pp}$ and f = 1 kHz	Macro-DBD (Ref. 1) $F_x = 120$ mN/m $P_{avg} = 590$ W/m $V = 74\,kV_{pp}$ and f = 1 kHz	Macro-DBD (Ref. 4) $v_{max} = 1.4$ m/s and $F_x = 3.9$ mN/m $P_{avg} = 20$ W/m $V = 20\,kV_{pp}$ and f = 1 kHz	Macro-DBD (Ref. 9) $v_{max} = 2$ m/s $P_{avg} = 25$ W/m $V = 24\,kV_{pp}$ and f = 1 kHz
Thrust 'Effectiveness' (mN/W)	0.20	0.20	0.20	—
Thrust density (mN/m^3)	5.29×10^6	2.57×10^5	6.84×10^4	—
Thrust per actuator mass	0.215	9.70×10^{-3}	4.10×10^{-3}	—
Velocity 'Effectiveness' (m/s)/(W/m)	0.13	—	0.07	0.08
Vel. per actuator volume $(m/s)/m^3$	3.53×10^6	—	2.46×10^4	9.52×10^4
Vel. per actuator mass (m/s)/g	1.41	—	1.44×10^{-2}	7.60×10^{-2}
Actuator efficiency	4.00×10^{-4}	—	2.73×10^{-4}	—

microscale dimensions. Devices that were operated at $5\,kV_{pp}$ and 1 kHz consumed 15 W/m on average. The power consumption scales with $V^{3.5}$ indicating that the microscale devices follow similar power trends to macroscale DBD actuators.[8] The reduction in power is attributed to the reduction in the necessary breakdown voltage for discharge gained from using a thin dielectric layer. The fluid velocities reached 2.0 m/s and the thrust was up to 3 mN/m. The actuator "effectiveness"–output per consumed power–was used to compare microscale and macroscale DBD actuator thrust and velocity with power consumption. The microscale actuators demonstrate equal thrust effectiveness to macroscale devices, indicating that the DBD actuator thrust performance scales linearly with size reduction. The velocity effectiveness of microscale actuators is 63%–86% greater than that of macro DBD actuators. In one case, the microscale actuator demonstrated 31% higher energy conversion efficiency compared to the macroscale actuator. Overall, the microscale DBD actuator induced velocity, thrust, and power consumption scale favorably with size reduction. The compact size and low mass of the micro actuators make them implementable with minimal weight penalty.

This work was partially supported through AFOSR Grant monitored by Dr. Douglas Smith, through NSF I/UCRC program and through a grant from the Florida Center for Advanced Aero-Propulsion. The second author is also supported by a DOD SMART scholarship. The authors also gratefully acknowledge the assistance from the staff of the UF Nanoscale Research Facility.

[1]F. O. Thomas, T. C. Corke, M. Iqbal, A. Kozlov, and D. Schatzman, AIAA J. **47**, 2169 (2009).
[2]F. F. Chen, *Introduction to Plasma Physics and Controlled Fusion Plasma Physics* (Springer, 1984).
[3]C. C. Wang and S. Roy, J. Appl. Phys. **106**, 013310 (2009).
[4]T. Abe, Y. Takizawa, S. Sato, and N. Kimura, AIAA J. **46**, 2248 (2008).
[5]A. R. Hoskinson, N. Hershkowitz, and D. E. Ashpis, J. Phys. D: Appl. Phys. **41**, 245209 (2008).
[6]J. C. Zito and D. P. Arnold, in *Tech. Dig. Solid-State Sensors, Actuators, and Microsystems Workshop*, Hilton Head NC, 6–10 June 2010 (Transducer Research Foundation, 2010), pp. 238–241.
[7]M. Gamero-Castano, Rev. Sci. Instrum. **74**, 4509 (2003).
[8]C. L. Enloe, T. E. McLaughlin, R. D. VanDyken, K. D. Kachner, E. J. Jumper, and T. C. Corke, AIAA J. **42**, 589 (2004).
[9]M. Forte, J. Jolibois, J. Pons, E. Moreau, G. Touchard, and M. Cazalens, Exp. Fluids **43**, 917 (2007).
[10]V. I. Gibalov and G. Pietsch, J. Phys. D: Appl. Phys. **33**, 2618 (2000).